Electronic structure and valence-band spectra of $FeBO_3$

A. V. Postnikov,* St. Bartkowski, M. Neumann, and R. A. Rupp
Fachbereich Physik, Universität Osnabrück, D-49069 Osnabrück, Germany

E. Z. Kurmaev, S. N. Shamin, and V. V. Fedorenko
Institute of Metal Physics, Russian Academy of Sciences–Ural Division, 620219 Yekaterinburg, GSP-170, Russia
(Received 31 May 1994)

Based on *ab initio* electronic-structure calculations by the linear muffin-tin orbital method and the combined analysis of x-ray photoelectron and x-ray B $K\alpha$, O $K\alpha$, and Fe $L\alpha$ emission spectra in a common energy scale, the aspects of hybridization within the valence band of $FeBO_3$ are discussed in detail. X-ray photoelectron spectra of B_2O_3 and H_3BO_3 have also been obtained and are discussed in comparison with that of $FeBO_3$.

I. INTRODUCTION

There are only two crystals known which are magnetically ordered above 300 K and transparent in parts of the visible spectrum: FeF_3 and $FeBO_3$. Single crystals of $FeBO_3$ were first grown in 1963,[1] which stimulated a great number of investigations of magnetic, optical, and magneto-optical properties, and applications of this material.[2] In spite of the considerable practical interest in macroscopic properties, the underlying microscopic electronic structure of $FeBO_3$ seems to be rather poorly studied by experimental or theoretical means. The electronic transitions have been discussed[2] based on a simple molecular orbital theory of Fe^{3+} ions put into a trigonally distorted $O_6{}^{2-}$ octahedron.[3] There were, to our knowledge, no first-principles electronic structure calculations presented for this material so far, nor experimental investigation of the valence-band structure by spectroscopic methods.

In this paper, we present the results of band structure calculations for bulk $FeBO_3$ along with the experimental x-ray photoelectron spectra (XPS) of the valence band and core levels and with the x-ray emission Fe $L\alpha$, B $K\alpha$, and O $K\alpha$ spectra which probe the energy distribution of different partial densities of states (DOS's) in the valence band. Taken together, these experimental techniques allow one to bring different emission spectra to the same energy scale and to extract essential information about the chemical bonding and electronic structure of $FeBO_3$, whereas the parameter-free analysis of the band structure creates a basis for subsequent theoretical investigation of optical and magneto-optical properties.

II. EXPERIMENT

XPS spectra were measured using an ESCA spectrometer of Perkin-Elmer (PHI 5500 ci, monochromatized Al $K\alpha$ radiation). The single crystal of $FeBO_3$ was cleaved in high vacuum and then immediately investigated so that any influence of adsorbed residual gas on the recorded photoelectron spectrum was avoided. XPS spectra were calibrated using the C 1*s* signal of hydrocarbon [E_B(C 1*s*)=284.6 eV]. In case of B_2O_3 and H_3BO_3, pressed pellets were used as samples, and were also cleaved in high vacuum.

X-ray emission spectra Fe $L\alpha$ (2*p*-3*d*4*s* transition) and O $K\alpha$ (1*s*-2*p* transition) were registered by an electron-probe JCXA-733 microanalyzer with a fully focused Johan type spectrometer [crystal analyzer of TAP (thallium phtalate, $C_8H_5O_4Tl$), $2d$=25.76 Å, curved to R=280 mm]. The energy resolution was 2.5 and 0.5 eV, respectively. The B $K\alpha$ (1*s*-2*p* transition) x-ray emission band was studied using a small-spot x-ray spectrometer with a diffraction grating[4] (N=600 lines/mm, R=2 m) with energy resolution ΔE=1.7 eV.

All emission spectra have been brought to the same energy scale with respect to the Fermi level using the binding energies of relevant initial (core level) states of the x-ray transitions as measured by the XPS technique. Corresponding binding energies are 711.5 eV (Fe 2*p*); 191.8 eV (B 1*s*); 531.1 eV (O 1*s*). Each spectrum has been arbitrarily normalized to its maximum.

III. ELECTRONIC STRUCTURE CALCULATIONS

$FeBO_3$ is known to crystallize in space group $R\bar{3}c$-D_{3d}^6 (No. 167 of the International Tables) with two formula units per unit cell.[2,5] The lattice constants in the hexagonal setting are a=4.626(1) Å, and c=14.493(6) Å. The crystal structure is formed by interchanged planes of BO_3 groups and Fe atoms, the latter being centered in slightly distorted O_6 octahedra. We performed the band structure calculation within the local spin density formalism, making use of the tight-binding linear muffin-tin orbital method in the atomic sphere approximation.[6] Since the crystal structure of $FeBO_3$ is rather loosely packed, we had to introduce empty spheres to provide the optimal space filling. The positions of atoms and the empty spheres (22 in total) along with their relative sizes (in terms of the average Wigner-Seitz radius w=1.872 a.u.) are specified in Table I. The sphere sizes have been chosen so as to provide minimal overlap and good matching

TABLE I. Atomic coordinates and atomic sphere radii used in the calculation.

	No. of positions	Wyckoff notation	S/w
Fe	2	b	1.589
B	2	a	0.9
O	6	e (x=0.548)	0.85
$E1$	6	e (x=0.952)	0.85
$E2$	6	d	0.95

of potential at the sphere boundaries. The internal coordinate x determining the position of oxygen atoms corresponds to the B-O bond length of $0.2981a$, as determined by Diehl.[5] Since this value is close to 1/3, the introduction of empty spheres $E1$ at the positions symmetric to those of O with respect to B in the BO_3 groups creates almost perfect hexagonal close packing within the B-O planes. Missing positions in this packing apart from the BO_3 groups are partially filled by larger Fe spheres approaching from above and below the B-O plane. Another set of empty spheres $E2$ improves the packing within the Fe planes.

For the tetrahedron integration, we used a mesh with up to 10×10×10 divisions over the full Brillouin zone (172 inequivalent **k** points). We have found such a mesh sufficiently dense to achieve the convergence of the total energy in the number of **k** points within 0.5 mRy, which enabled a reliable comparison of the relative stability of different magnetic phases. Partial DOS's presented below are also calculated with such a mesh.

Magnetic moments on Fe atoms in $FeBO_3$ at positions (000) and $(\frac{1}{2}\frac{1}{2}\frac{1}{2})$ of the rhombohedral unit cell are known to order nearly antiferromagnetically in the (111) plane, i.e., the plane of easy magnetization. Therefore the symmetry allows—in contrast to the isostructural $FeCO_3$ in which the spins are parallel to the [111] axis—the antisymmetric Dzialoshinsky-Moriya exchange, resulting in a small canting (about 0.9°) of spins, and thus in weak ferromagnetism. Both the antiferromagnetic sublattice magnetization and the net ferromagnetic magnetization are perpendicular to the crystallographic c axis and nearly perpendicular to each other.[7]

In order to study the effect of the magnetic ordering on the electronic structure, we performed our calculations for ideally ferromagnetic (FM) and antiferromagnetic (AFM) phases, neglecting the canting of magnetic moments. Since our calculations did not incorporate the spin-orbit interaction, the orientation of magnetic moments with respect to the crystal lattice was not specified.

IV. DISCUSSION

Calculated electron bands for AFM $FeBO_3$ are shown in Fig. 1, and partial DOS's within B and O atomic spheres in Fig. 2. Spin-resolved partial DOS of B and O and correspondingly partial charges within their atomic spheres are practically unaffected by the magnetic ordering, as can be seen from Table II; magnetic moments are essentially confined to the Fe $3d$ shell. They are, according to our calculation, considerably underestimated as compared to the observed value of $4.70\mu_B$.[8]

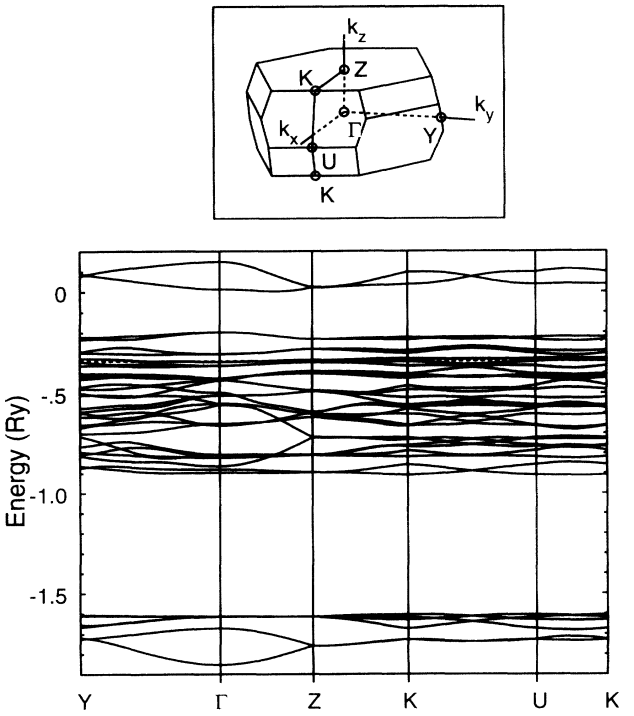

FIG. 1. Brillouin zone and energy bands in antiferromagnetic $FeBO_3$.

The partial Fe $3d$ DOS for the FM structure, which exhibits the most pronounced differences as compared to the AFM phase, is shown in Fig. 3, and the total DOS's for both types of magnetic order are presented in Fig. 4. The total energies for FM and AFM structures are, respectively, −6089.460 and −6089.466 Ry. However tiny, the difference is stable against the refinement of the **k**-

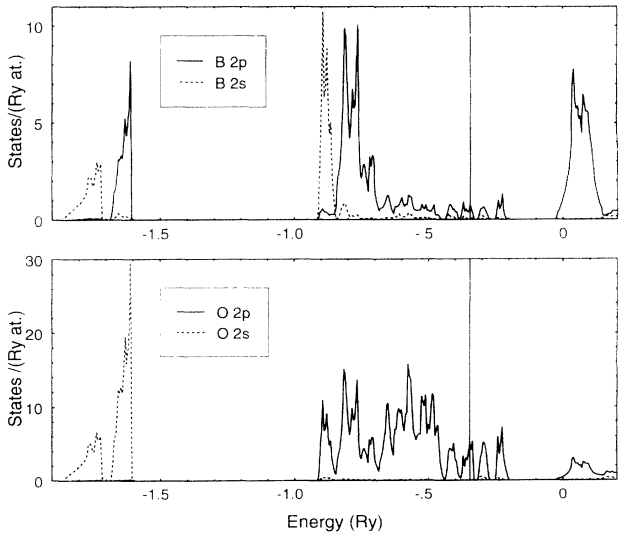

FIG. 2. Partial B and O DOS's in antiferromagnetic $FeBO_3$.

TABLE II. Charges within atomic spheres in two magnetic settings of $FeBO_3$.

	Fe	B	O	$E1$	$E2$
			Ferromagnetic structure		
$s\uparrow$	0.31	0.29	0.68	0.12	0.17
$s\downarrow$	0.30	0.29	0.68	0.12	0.16
$p\uparrow$	0.52	0.56	1.74	0.11	0.16
$p\downarrow$	0.51	0.56	1.70	0.11	0.15
$d\uparrow$	3.81	0.12	0.01	0.06	0.08
$d\downarrow$	3.01	0.12	0.01	0.06	0.08
Total	8.46	1.94	4.82	0.58	0.80
M (μ_B)	0.82	0.00	0.04	0.00	0.02
			Antiferromagnetic structure[a]		
$s\uparrow$	0.31	0.58	1.33	0.24	0.17
$s\downarrow$	0.30				0.17
$p\uparrow$	0.51	1.12	3.46	0.23	0.16
$p\downarrow$	0.51				0.16
$d\uparrow$	3.91	0.24	0.03	0.11	0.07
$d\downarrow$	2.92				0.07
Total	8.46	1.94	4.82	0.58	0.80
M (μ_B)	1.00	0.00	0.00	0.00	0.00

[a]Fe and $E2$ sites are split into two sets with opposite magnetization; B, O, and $E2$ are nonmagnetic by symmetry.

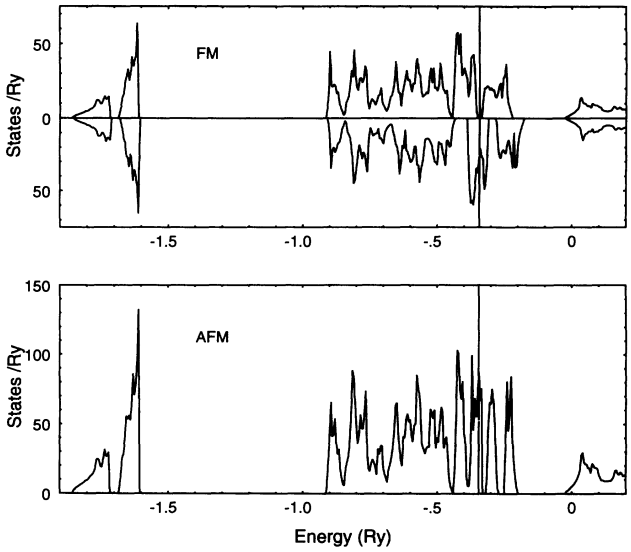

FIG. 4. Total DOS (including higher states and contributions from empty spheres, per formula unit) in ferromagnetic and antiferromagnetic $FeBO_3$.

space integration grid. The AFM structure was found therefore to be more stable, in agreement with experiment.

Calculated partial charges within atomic spheres have only limited value as a measure of charge transfer, because they are of course strongly determined by our chosen partitioning of space. Nevertheless, the considerable amount of charge accumulated within empty spheres indicates that the chemical bonding in $FeBO_3$ is generally of covalent rather than ionic character. A non-negligible fraction of the charge density of d symmetry within the B spheres is due to sp^2 hybridized orbitals mediating B-O covalent bonding which cannot be sufficiently described by the spherical harmonics expansion with $l = 0$ and 1. On the contrary, p states on the O sites essentially retain the $l = 1$ angular dependence, which leaves a very small charge contribution of the d symmetry within O spheres.

As is typical for many oxides, a comparatively narrow O $2s$ band lies by ~15 eV lower than the center of a broader valence band formed mostly by O $2p$ states hybridized with the states of other constituent atoms (B $2s2p$; Fe $4s4p$). Fe $3d$ states hybridize only slightly with this O $2p$–originating valence band; they are mostly represented by narrow peaks at the top of the latter. Between the Fe $3d$–related flat energy bands and the conduction band, mostly formed by B $2p$ states (with some admixture of Fe $4s4p$), the calculation indicates a gap of ~2.5 eV for the AFM structure and ~2.1 eV for the FM structure. The band gap obtained from the onset of the

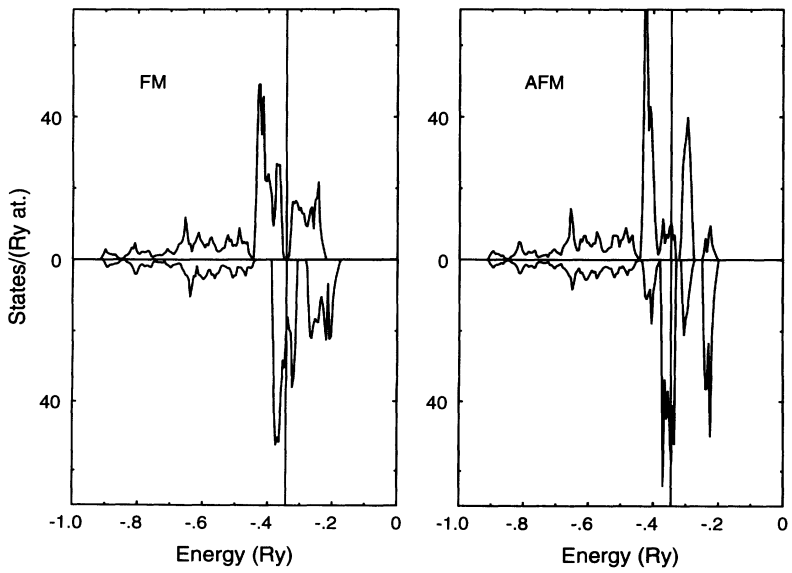

FIG. 3. Partial Fe $3d$ DOS in ferromagnetic and antiferromagnetic $FeBO_3$.

fundamental optical absorption edge, about 2.9 eV,[9] is slightly larger.

A peculiar feature of $FeBO_3$ is the splitting of the lower O $2s$–related band into two distinct subbands, separated by a gap. As can be seen from the distribution of partial DOS at the B site (Fig. 2), the lower subband results exclusively from the O $2s$–B $2s$ hybridization; the upper subband is due to the O $2s$–B $2p$ mixing. B $2s$ states manifest themselves also just at the bottom of the valence band as two energy bands with low dispersion, separated by an indirect gap from the main bulk bands.

The narrow Fe $3d$–related bands at the top of the valence band are split by the crystal field, and crossed by the Fermi level. (In the FM phase, the Fermi level falls into the gap between two crystal-field-split spin-up bands, but indeed crosses a spin-down band.) Therefore, according to our calculation $FeBO_3$ exhibits metallic behavior, whereas experimentally it is dielectric. A similar kind of discrepancy is known to occur in band structure calculations of $3d$ oxides based on a local density approximation, as has been discussed at length by, e.g., Terakura *et al.*[10] Actually, the local Fe $3d$ DOS according to our present calculation for $FeBO_3$ has many similarities with that calculated for FeO by Terakura *et al.*[10] Although the O_6 octahedra around Fe atoms in $FeBO_3$ are slightly distorted and the point group at the Fe site becomes D_{3d}, the symmetry-allowed splitting of the t_{2g} band into a_{1g} and e_g is very small, and two distinct peaks in the partial Fe $3d$ DOS for each spin direction can be referred to as representing t_{2g} and e_g subbands. The energy separation between them is $\sim$0.07 Ry, comparable to the value obtained in Ref. 10. As in Ref. 10, the Fermi level crosses the minority spin t_{2g} band; however, in $FeBO_3$ we found only the t_{2g} subband to be occupied for the majority spin but not e_g, thus resulting in considerably lower local magnetic moment.

The certain similarity of the local electronic structure at the Fe site in $FeBO_3$ with that in FeO helps also to understand the preference for the AFM type of ordering, as well as the narrower t_{2g} and e_g subbands in the AFM phase as compared with the FM one. In the AFM phase, the coupling mediated by p orbitals of oxygen atoms occupying shared corners of coupled FeO_6 octahedra is always between oppositely magnetized Fe atoms. Following the discussion of Ref. 10, one may understand that such Fe-O-Fe hybridization does not give rise to the broadening of t_{2g} and e_g subbands within each particular spin direction, in contrast to the situation in FM $FeBO_3$. A narrow band lowers the band energy, as can be seen from Fig. 3, and hence favors the AFM type of ordering. The observed noncollinearity of magnetic moments is probably related to the trigonal distortion of FeO_6 octahedra, as well as to the fact that they are coupled to form a loose trigonal structure rather than packed into a compact fcc lattice as in $3d$ oxides.

The importance of taking into account the Coulomb correlation effects in order to lift the degeneracy between occupied and empty states within the minority-spin t_{2g} subband has been briefly discussed in Ref. 10. A practical, however simplified, way of doing this by means of the so-called unoccupied-states potential correction to the local density functional[11] resulted indeed in opening the gap in the minority-spin subband of FeO, thus providing the correct description of this material as an insulator. At the same time, the magnitude of the magnetic moment was considerably enhanced. Based on the simple quantitative analysis of the tendency towards lifting the orbital degeneracy within the minority-spin t_{2g} subband in FeO,[10] and on the fact that the calculated local Fe $3d$ DOS at the Fermi level in $FeBO_3$ is even slightly higher than in FeO, one should expect that the appropriate scheme including the Coulomb correlation within the Fe $3d$ shell, like, e.g., local density approximation (LDA)+U,[12] will result in opening the gap in $FeBO_3$ as well. This may also dramatically enhance the magnetic moment, as was shown for Fe impurities in MgO.[13] Such a correction is essential, e.g., for a realistic description of optical transitions and magnetooptical properties, but it is beyond the scope of the present paper where we concentrate on the ground state properties, or—as far as XPS is concerned—on the analysis of the chemical bonding which manifests itself in the particular form of the valence band.

The XPS valence-band spectrum of $FeBO_3$, which provides, if we neglect the differences in atomic photoionization cross sections, information about the energy distribution of the total density of states (DOS), is shown in the top of Fig. 5 in comparison with Fe $L\alpha$, B $K\alpha$, and O $K\alpha$ x-ray emission spectra which probe partial Fe $3d$, B $2p$, and O $2p$ DOS, respectively. The calculated total DOS, broadened with the width parameter 0.7 eV, is shown in Fig. 5 at the bottom.

As is seen from Fig. 5, the energy of the low-energy subband of B $K\alpha$ XES is close to that of the e feature of the XPS valence-band spectrum which has O $2s$ character. This indicates the appreciable B $2p$–O $2s$ hybridization, as supported by the results of band structure calculation.

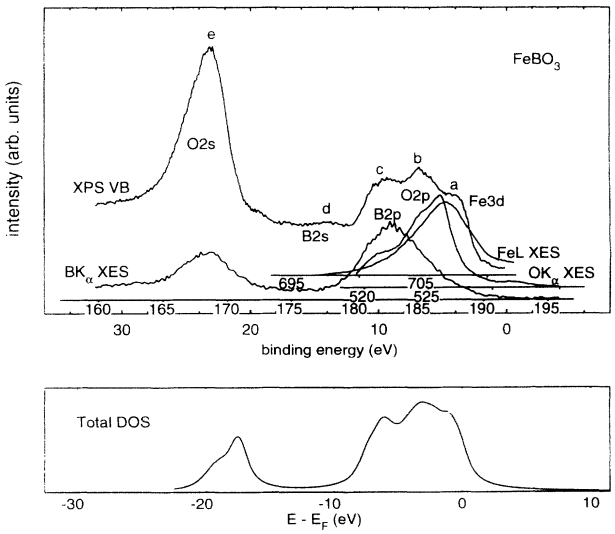

FIG. 5. X-ray photoelectron spectrum of the valence band, O $K\alpha$, B $K\alpha$, and Fe $L\alpha$ x-ray emission spectra (XES) (top) and calculated total DOS, broadened with the width parameter 0.7 eV (bottom), of $FeBO_3$.

The next *d* feature (B 2*s*) of XPS has no corresponding feature in B $K\alpha$ XES, which means (also in agreement with band structure calculations) that the B 2*s*–B 2*p* hybridization is negligible in $FeBO_3$. Unfortunately, the use of the TAP crystal analyzer in our XES measured at JCXA-733 put a limit on the low-energy wavelength at the photon energy 521.5 eV, which resulted in some cutoff of the low-energy tails of the O $K\alpha$ XES. Because of this experimental limitation, we could not check the prediction of theory in regard to the B 2*s*–O 2*p* hybridization in the valence band of $FeBO_3$.

We have found a strong overlap of B $K\alpha$ and O $K\alpha$ XES and the coincidence of their maxima with those of the valence-band XPS, which indicates a strong B 2*p*–O 2*p* hybridization. The same conclusion follows from the analysis of partial DOS's obtained in the calculation (Fig. 2). It was found that the maximum of intensity of the Fe $L\alpha$ XES is close to the *a* feature of the valence-band XPS, which means that the Fe 3*d* states are concentrated mainly at the top of the valence band of $FeBO_3$.

It is noteworthy that the valence-band XPS of $FeBO_3$ is quite similar to the spectra of H_3BO_3 and B_2O_3 (Fig. 6). The same holds for B $K\alpha$ XES of these compounds.[14] It means that the electronic structure of H_3BO_3 and B_2O_3 is practically identical.

For B_2O_3, we have studied also B $K\alpha$ and O $K\alpha$ XES. The XPS valence-band spectrum of B_2O_3 was brought onto a common energy scale with B $K\alpha$ and O $K\alpha$ XES in Fig. 6 in the same way as described above for $FeBO_3$, making use of the core level binding energies measured by XPS. For B_2O_3, the binding energies are 191.3 eV (B 1*s*) and 531.2 eV (O 1*s*). We used the same notation for the features of the valence-band XPS as in Fig. 5. It was found (as in the case of $FeBO_3$) that the low-energy *e* subband of XPS is formed by O 2*s* (B 2*p*) states. The next *d* feature is mainly of B 2*s* character, and at the top of the valence band (*c*–*b*), strongly hybridized O 2*p*–B 2*p* states prevail.

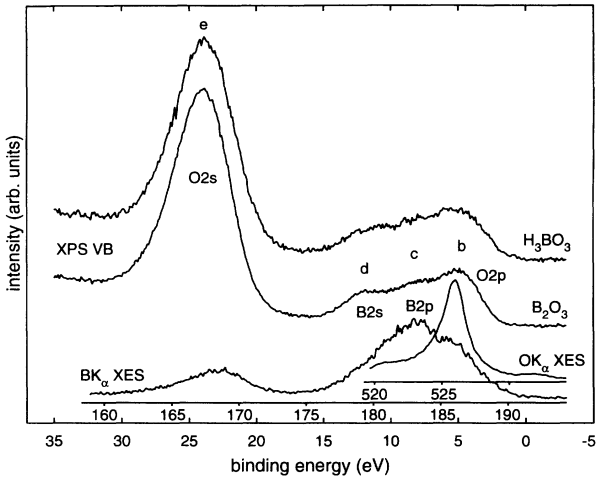

FIG. 6. X-ray photoelectron spectra of the valence band of H_3BO_3 (upper curve) and B_2O_3; O $K\alpha$ and B $K\alpha$ x-ray emission spectra in B_2O_3.

V. CONCLUSION

In the present paper, we report, to our knowledge for the first time, first-principles calculations of the electronic structure of $FeBO_3$ along with x-ray emission and x-ray photoelectron spectroscopy measurements. The combination of both experimental techniques and comparison with theory enabled us to obtain detailed information as to the structure of the valence band and the underlying hybridization. We could explain why magnetic moments on Fe sites are ordered antiferromagnetically. In order to analyze properties other than those of the ground state, like, e.g., optical and magneto-optical behavior, the incorporation of Coulomb correlation effects beyond the local density approximation was found to be essential.

ACKNOWLEDGMENTS

Financial support of the Deutsche Forschungsgemeinschaft (SFB 225, Graduate College) is gratefully acknowledged.

* On leave from Institute of Metal Physics, Russian Academy of Sciences, Yekaterinburg, Russia. Electronic address: apostnik@physik.uni-osnabrueck.de

[1] I. Bernal, C. W. Struck, and J. G. White, Acta Crystallogr. **16**, 849 (1963).
[2] R. Diehl, W. Jantz, B. J. Noläng, and W. Wettling, Curr. Top. Mater. Sci. **11**, 241 (1984).
[3] S. Krupicka, *Physik der Ferrite und der verwandten magnetischen Oxide* (Vieweg, Braunschweig, 1973).
[4] E. Z. Kurmaev, V. V. Fedorenko, S. N. Shamin, A. V. Postnikov, G. Wiech, and Y. Kim, Phys. Scr. **T41**, 288 (1992).
[5] R. Diehl, Solid State Commun. **17**, 743 (1975).
[6] O. K. Andersen and O. Jepsen, Phys. Rev. Lett. **53**, 2571 (1984); O. K. Andersen, Z. Pawlowska, and O. Jepsen, Phys. Rev. B **34**, 5253 (1986).
[7] M. Eibschütz and M. E. Lines, Phys. Rev. B **7**, 4907 (1973).
[8] M. Pernet, D. Elmaleh, and J.-C. Joubert, Solid State Commun. **8**, 1583 (1970).
[9] I. S. Edelman, A. V. Malakhovskii, T. I. Vasileva, and V. N. Seleznev, Fiz. Tverd. Tela (Leningrad) **14**, 2810 (1972) [Sov. Phys. Solid State **14**, 2442 (1973)].
[10] K. Terakura, T. Oguchi, A. R. Williams, and J. Kübler, Phys. Rev. B **30**, 4734 (1984).
[11] V. I. Anisimov, M. A. Korotin, and E. Z. Kurmaev,

J. Phys. Condens. Matter **2**, 3973 (1990).
[12] V. I. Anisimov, I. V. Solovyev, M. A. Korotin, M. T. Czyzyk, and G. Sawatzky, Phys. Rev. B **48**, 16 929 (1993).
[13] M. A. Korotin, A. V. Postnikov, T. Neumann, G. Borstel, V. I. Anisimov, and M. Methfessel, Phys. Rev. B **49**, 6548 (1994).
[14] R. C. Ehlert and R. A. Mattson, Adv. X-Ray Anal. **9**, 456 (1965).